IEEE Access
Multidisciplinary | Rapid Review | Open Access Journal

Received February 5, 2019, accepted February 17, 2019, date of publication February 21, 2019, date of current version March 7, 2019.

Digital Object Identifier 10.1109/ACCESS.2019.2900668

The Impact of Bushing Thickness on the Piston/Cylinder Interface in Axial Piston Pump

JIANG JIHAI[1], WANG KELONG[1], WANG ZEBO[1], AND SUN YI[2]

[1]Harbin Institute of Technology, Harbin 150001, China
[2]Beijing Institute of Precision Mechatronics and Control Equipment, Beijing 100076, China

Corresponding author: Wang Kelong (wang.kelong1985@gmail.com)

This work was supported in part by the National Natural Science Foundation of China under Grant 51275123, in part by the National Key Technology R&D Program under Grant 2014BAF08B06, and in part by the Major National Scientific and Technological Achievements Transformation Project.

ABSTRACT A comprehensive multi-domain simulation tool that could predict the lubricating flow between piston and bushing in the cylinder is presented in this paper. The first module simulates the main flow through the piston pump according to a lumped parameter model. The estimation of instantaneous pressure in each displacement chamber is utilized in another module dedicated to the prediction of the lubricating gap flow between piston and bushing. This lubricating gap flow module is a numerical model based on the fluid-structure interaction algorithm in which the fluid film pressure is calculated by the Reynolds equation. The oil film height is determined by the micromotions of the piston and the deformation of both the piston and bushing interface. The micromotions of the piston are obtained from the dynamic force balance of external force and fluid force. Influence method is applied to calculate the deformations of piston and bushing, which is an efficient offline method. With different thicknesses of the bushing, the power loss and the leakage of the piston/cylinder interface are compared. The test rig is built to measure the friction power loss of piston. The results highlight the impact of the bushing on the piston/cylinder lubricating interface. The mathematical model proposed in this paper has the potential to be a theoretical guide for the optimal design of an axial piston pump.

INDEX TERMS Hydraulic drives, axial piston pump, bushing, piston/cylinder interface, fluid structure interaction.

I. INTRODUCTION

As a key component in hydraulic system, axial piston pumps with swash plate design are widely used in hydrostatic transmission equipment for their benefits of high efficiency and power density [1]. Main components of axial piston pump is shown in Fig. 1. Usually, odd number of pistons are uniformly distributed on cylinder. The cylinder is connected and rotates with pump shaft. Pistons rotate around pump shaft and reciprocate along y direction due to the tilt of swash plate, which realize the variation of displacement chamber volume. Valve plate is used to distribute and transfer the inlet and outlet oil. Piston/cylinder lubricating interface which fulfils bearing and sealing functions simultaneously, is one of the most critical part of axial piston pump design. It is a main source of viscous friction and leakage power loss in axial piston pump. Several measures are taken to improve the wear resistance of piston/cylinder interface, such as copper alloy bushing, grooves and micro-shapes on piston. Bushing is one of the most effective way in industrial application. However, the thickness of bushing is mainly determined

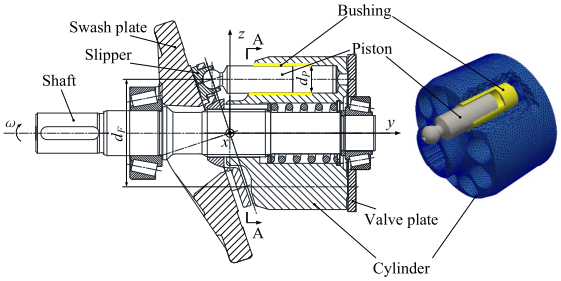

FIGURE 1. Main components in axial piston pump.

The associate editor coordinating the review of this manuscript and approving it for publication was MENGMENG LI.

through experience and experiment, which are at low efficiency and high cost. The keystone of this study is the numerical model of piston/cylinder interface, aiming to be a theoretical guide for the structural parameter selection of piston/cylinder interface.

The analysis of piston/cylinder interface is always a hot topic, and most researches try to reveal the lubrication mechanism and improve its performance and reliability. Yamaguchi [2] analyzed the motion of piston and solved Reynolds equation with rigid piston. The metallic contacts are also introduced. Harris *et al.* [3] studied the impact of spin motion of piston on the oil film between piston and cylinder. Tanaka *et al.* [4], [5] analyzed the characteristics of piston/cylinder lubrication interface and tested their theories experimentally. However, the micro motion and dynamic loads of piston are neglected in those models. Manring [6] developed a mathematical model that could describe the friction between piston and cylinder with Stribeck curve. Li *et al.* [7] introduced an artificial leakage into axial piston pump and simulated its leakage. Numerical model becomes an effective method to predict the performance of piston/cylinder interface with the development of computer science. Wieczorek and Ivantysynova [8] developed a mathematical simulation tool -CASPAR, which can be used to predict the micro motion and pressure distribution of rigid piston/cylinder interface in axial piston pump. Pelosi and Ivantysynova [9]–[11] developed a fluid-structure interaction (FSI) model and introduced the deformation of piston/cylinder interface. Kumar and Bergada [12] introduced a mathematical model with grooves being cut on piston. Xu [13], [14] and Jiang and Wang [15] investigated the pressure distribution and micro-motion of piston. Wondergem and Ivantysynova [16], [17] focused on the micro surface shapes of piston and studied their impact on the performance on piston cylinder interface. Those research tries to predict the oil film performance but the copper alloy bushing between piston and cylinder is not taken into consideration.

The FSI numerical model for the piston/cylinder interface with bushing is developed for the first time in this paper and the impact of bushing thickness on piston/cylinder interface is analyzed. The dynamic pressure in displacement chamber is calculated with the main flow model. Reynolds equation [18] is solved on oil film mesh and the pressure distribution is obtained. The deformation of both the piston and the bushing are considered because of their effects on the oil film gap height and the pressure distribution. Finally, the performances of piston/cylinder interface with different bushing thicknesses are compared. Fig. 2 shows the multi domain simulation tools developed for the piston/cylinder interface in this study. The main flow model is built on the working condition and geometrical model. Then the dynamic loads in displacement chamber and some other initial conditions for piston/cylinder interface are obtained. The FSI model of piston/cylinder interface is developed with OpenFoam which includes fluid solver, structure solver, and the interaction between these two fields.

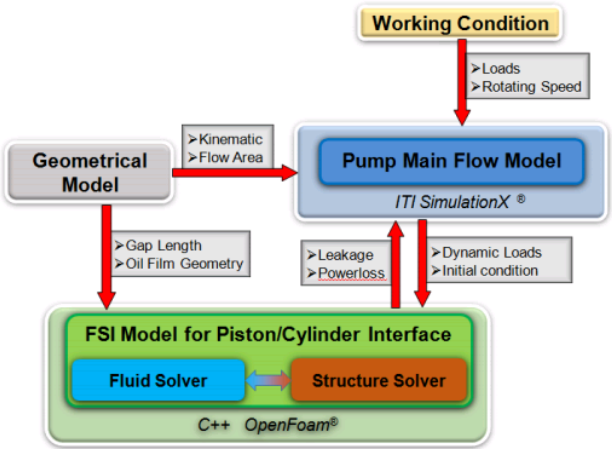

FIGURE 2. Framework of multi domain simulation tools.

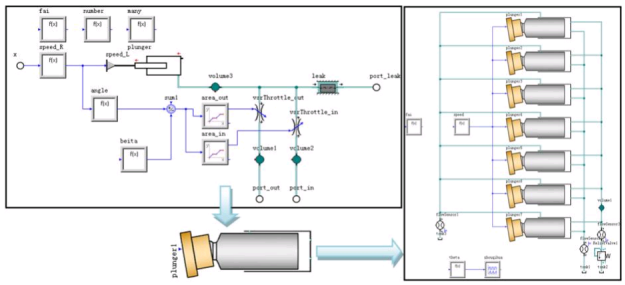

FIGURE 3. Pump main flow model.

II. SIMULATION OF DYNAMIC PRESSURE IN DISPLACEMENT CHAMBER

The main flow model assumes the suction and delivery volumes in cylinder as separate control volumes. The displacement is connected with the high and low pressure port alternately. The flow area between them is set according to the structure of valve plate. A single piston chamber model is developed, and after compounding it as a new component the simulation model for the whole pump is built and shown in Fig. 3.

The pressure built-up equation for the dynamic pressure in displacement chamber are described as:

$$\frac{dp_{DC,i}}{dt} = \frac{E_F}{V_{DC,i}}\left[-\frac{dV_{DC,i}}{dt} - \left(Q_{HP,i} + Q_{LP,i} + Q_{leakage,i}\right)\right] \tag{1}$$

where E_F is the bulk modulus of the hydraulic oil. Usually, there are nine piston chambers in an axial piston pump and i is the index of piston chamber. $V_{DC,i}$ is the volume of displacement chamber. $Q_{leakage,i}$ is the leakage from the displacement chamber. $Q_{HP,i}$ and $Q_{LP,i}$ represent the flowrate from high pressure port and low pressure port to displacement chamber,

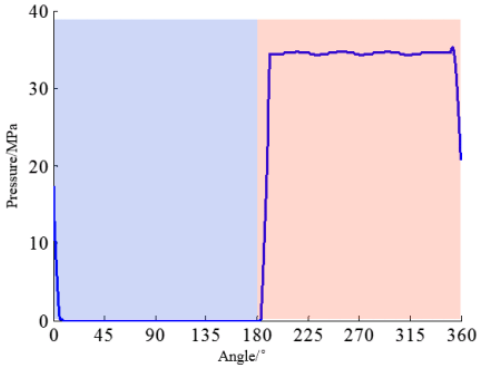

FIGURE 4. Dynamic pressure of displacement chamber.

which are calculated based on the orifice flow equation as:

$$Q_{HP,i} = C_d A_{HP,i} \sqrt{\frac{2}{\rho}\left(p_{\mathrm{DC},i} - p_{HP}\right)} \tag{2}$$

$$Q_{LP,i} = C_d A_{LP,i} \sqrt{\frac{2}{\rho}\left(p_{\mathrm{DC},i} - p_{LP}\right)} \tag{3}$$

After running the main flow model, the dynamic pressure in displacement chamber is obtained, which is an important boundary condition for the oil film between piston and bushing. The dynamic pressure through one revolution of pump shaft is shown in Fig. 4. For the first semi-cycle, the displacement chamber is sucking oil. Once the displacement passed 180°, it begins to pumping oil and a high pressure with pulsation is generated.

III. FSI MODEL OF PISTON/CYLINDER INTERFACE

A. SOLUTION ALGORITHM FOR FSI MODEL OF PISTON/CYLINDER INTERFACE

The FSI model of piston/cylinder interface is introduced in this section which includes fluid solver and structure solver. The algorithm designed for this study is shown in Fig. 5.

360 angle step is set in one revolution of pump shaft. For each angle, the piston position is calculated according to position and squeeze velocity of the previous angle and from which the gap height distribution of oil film is obtained. Then Reynolds equation is solved to get the pressure distribution. Deformation of both piston and bushing on each mesh cell is calculated based on the pressure distribution. Force balance of piston is checked and a proper squeeze velocity is found. The numerical model then goes to next step. The numerical model will not stop until the eccentricities of piston between revolutions are converged

B. FLUID SOLVER

Fig. 6 shows the gap between piston and bushing. A local coordinate $x_C - y_C - z_C$ is used. An eccentricity vector $\{e_{1x}, e_{1z}, e_{2x}, e_{2z}\}$ is defined to descript the position of piston since the micro motion of the piston has four degrees of freedom. They are the coordinates of the two special section

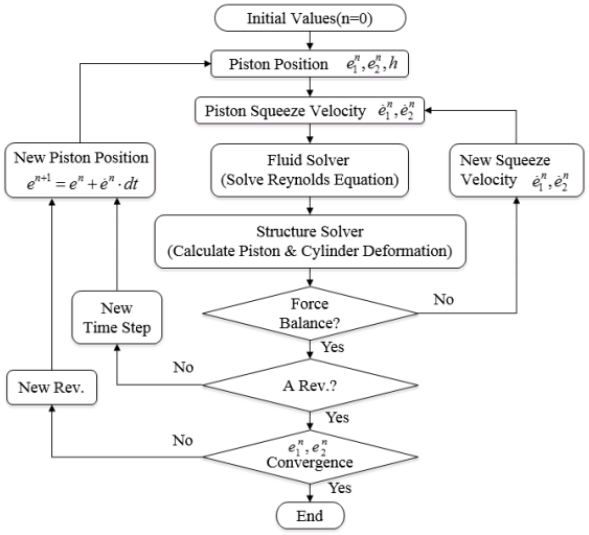

FIGURE 5. Solution algorithm for piston/cylinder interface.

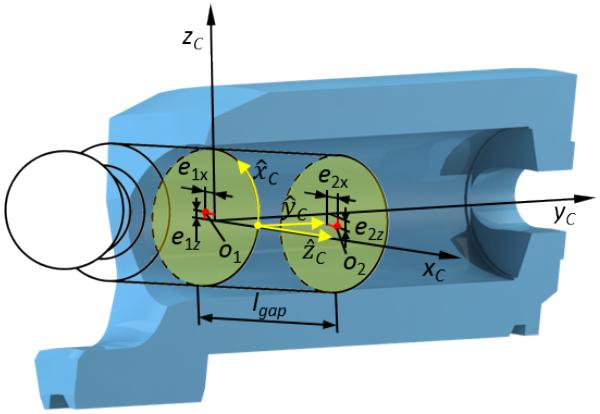

FIGURE 6. Piston position and eccentricity description.

centers that are located on the beginning and the end of piston/cylinder oil film. The coordinates of the other cutting planes on piston can be described as:

$$e_x|_{y_C} = (e_{2x} - e_{1x})\frac{y_C}{l_{gap}} + e_{1x} \tag{4}$$

$$e_z|_{y_C} = (e_{2z} - e_{1z})\frac{y_C}{l_{gap}} + e_{1z} \tag{5}$$

The oil film is unwrapped to a plane [19] for the convenience of numerical calculation. Another coordinate $\hat{x}_c - \hat{y}_c - \hat{z}_c$ is used, in which $\hat{x}_c$ represents oil film width along circle direction, $\hat{y}_c$ represents oil film length and $\hat{z}_c$ represents oil film thickness. Then based on the eccentricity vector of piston, the oil film thickness is calculated from:

$$\hat{z}\left(\hat{x},\hat{y}\right) = \sqrt{\left(r_p\cos\left(\hat{x}/r_p\right) - e_x|_{y_C}\right)^2 + \left(r_p\sin\left(\hat{x}/r_p\right) - e_z|_{y_C}\right)^2} - r_p + \Delta h \tag{6}$$

where Δh denotes the contribution to the fluid film thickness due to the surface elastic deformation of piston and cylinder, which is discussed later. The diagram of fluid mesh and boundary is shown in Fig. 7. Since the oil film is unwrapped,

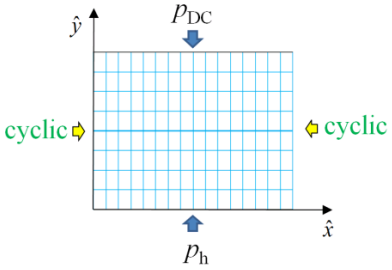

FIGURE 7. Diagram of fluid mesh and boundary conditions.

a 2-D mesh is created. The dynamic pressure calculated from main flow model is a boundary condition for oil film mesh. The downside boundary is applied the pump housing pressure. The left side and right side boundary are set to cyclic. The relative velocity between piston and cylinder is also applied to boundary.

The pressure distribution is obtained after Reynolds equation is solved on that fluid mesh, which is derived as follows:

$$\nabla\left(\frac{h^3}{12\mu}\nabla p\right) - \frac{v}{2}\nabla h - \frac{\partial h}{\partial t} = 0 \tag{7}$$

where h represents the thickness of oil film, including the gap height caused by the eccentricity vector of piston and the deformation of both piston and cylinder. v represents the relative velocity between piston and bushing. The first item in Reynolds equation means the flow due to pressure difference between boundaries. The second item distributes the hydrodynamic effect and the third one represents the squeeze effect. The leakage flow rate and viscous friction power loss are calculated with:

$$Q_{leakage} = \sum_{i=1}^{N_1} \vec{v}_i \vec{n}_i dA_i \tag{8}$$

$$P = \sum_{i=1}^{N} \vec{v}_i \vec{\tau}_{xy} dxdy \tag{9}$$

where N_1 is the cell number located on the downside boundary. N is the total cell numbers on the whole fluid mesh. $\vec{v}_i$ is the flow velocity of cell i and calculated based on the pressure distribution.

C. FORCE BALANCE CHECK

The forces acted on piston is shown in Fig. 8, which consist of external forces and fluid forces. The external forces include displacement chamber pressure force F_{DP}, the reaction force form swash plate F_{SN}, the friction force between slipper and swash plate F_{SF}, the force from retaining plate F_{RT}, the inertial force F_a and centrifugal force F_ω. The fluid forces are generated to achieve the balance of the piston, which include the fluid force on the normal direction F_{FN} and viscous friction force F_{FV}.

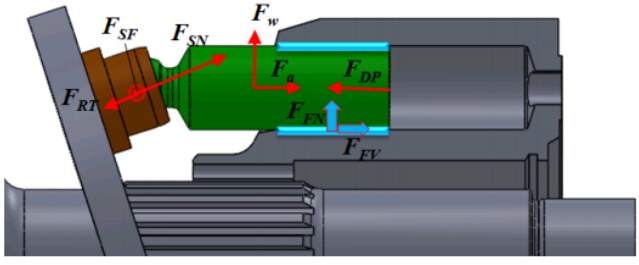

FIGURE 8. Force analysis of piston.

D. STRUCTURE SOLVER

The deformation of piston and cylinder affects the interface gap height, and finally changes the fluid field. Influence method, which is an efficient offline method for the elastic deformation, is implemented in this FSI model to calculate the deformation of both piston and cylinder. In this approach, two matrices are generated for piston and cylinder which stores the corresponding deformation with reference pressure p_{ref} applied to each of the individual cells. Since the deformation of piston and cylinder can be assumed to be of linear elasticity, after obtaining the oil film pressure distributio, the deformation of piston or cylinder is:

$$\delta h_i = \sum_{j=1}^{N_S} E_{ij} \frac{p_j}{p_{ref}} \tag{10}$$

where E_{ij} is the element of influence matrix E, which stroes the deformation of cell face j in the solid mesh with the reference pressure applied on cell face i. And p_j is the real pressure applied on cell face j. The process of influence matrix generation is finished with C++ and OpenFOAM library. The solid meshes of piston and cylinder are imported from ANSYS, which is made of unconstructed tetrahedral elements. Finite volume method is used to solve the deformation of each cell [20]:

$$\frac{\partial^2(\rho u)}{\partial t^2} - \nabla \cdot \left[\mu \nabla u + \mu (\nabla u)^T + \lambda Itr(\nabla u)\right] = \rho f \tag{11}$$

where μ and λ are the Lame's coefficients, relating to Young's modulus of elasticity E and Poisson's ratio υ. Since the Young's modulus E and Poisson's ratio υ of copper alloy and steel are different, the influence matrices should be different with materials. Also, the thickness, as the main parameters of copper alloy bushing, will affect the deformation. Fig. 9 shows the deformation under the same cell load with different bushing thickness. The valve of reference pressure P_{ref} is 1MPa.

In industrial application, the thickness of copper alloy bushing usually changes from 1mm to 2 mm. As can be seen from Fig. 9, with the increase of bushing thickness, the deformation under the same reference pressure increases. The max deformation with 2mm bushing is almost twice the cylinder without bushing.

Dynamic link between the fluid and solid mesh is built. The pressure field is obtained on the fluid mesh and the deformation is calculated on solid mesh. In order to realize the interaction between the fluid field and the structure field, a link is built. On the one hand, the pressure should be

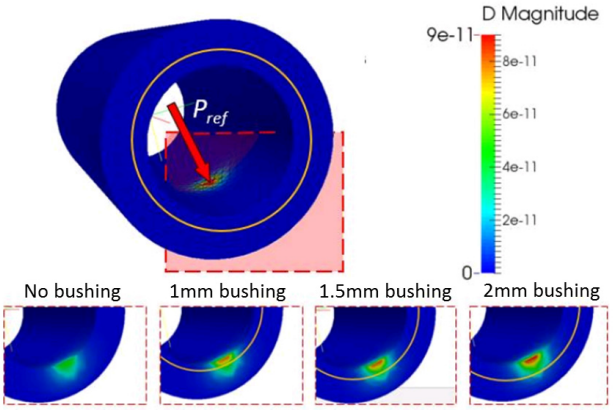

FIGURE 9. Deformation with different bushing thickness.

transferred to solid mesh to calculate the deformation of both piston and cylinder. On the other hand, the deformations are transferred to the fluid mesh, to solve the Reynolds equation with the deformed gap height. Fig. 10 shows the process of the linking of fluid mesh and solidmesh. As an example, for the solid mesh cell SC_1, according to its vertexes' coordinate, the fluid cells FC_1, FC_2, FC_3 and FC_4 are linked to SC_1. When the FSI model runs, the average pressure of FC_1, FC_2, FC_3 and FC_4 are transferred to SC_1. And after calculating deformation with influence matrix, the deformation of SC_1 will be transferred to FC_1, FC_2, FC_3 and FC_4. Besides, the fluid mesh changes along with the rotation of shaft, so this link will be built on every angle step.

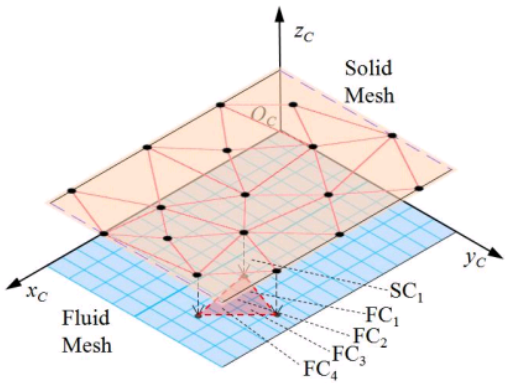

FIGURE 10. Dynamic link between solid and fluid mesh.

IV. RESULT

Since the dynamic pressure in displacement chamber is obtained and the FSI numerical model of piston/cylinder interface is built, some final results from those model could be calculated. Related parameters are reported in Table 1.

A. OIL FILM THICKNESS

The oil film thickness in one converged revolution is shown in Fig. 11, the clearance between piston and bushing 20μm and bushing thickness 1mm. Due to the micro motion of

TABLE 1. Parameters used in simulations.

Notation	Value	unit
d_P	17	mm
d_F	67	mm
ω	1500	rpm
C_d	0.63	-
ρ	860	kg/m^3
E_F	700	MPa
r_p	8.5	mm
μ	0.03	N·s/m^2
p_h	0.1	MPa
p_{HP}	35	MPa
p_{LP}	0.1	MPa

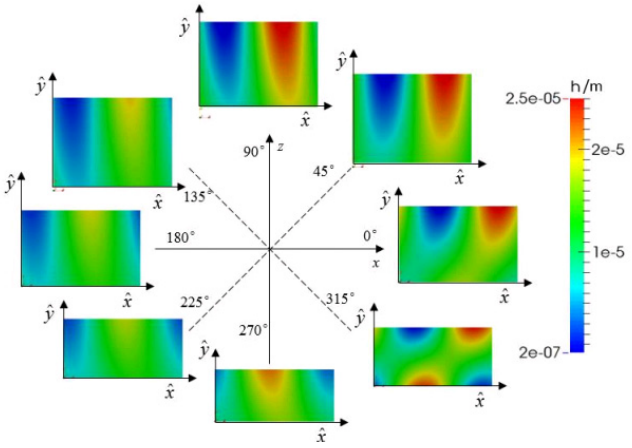

FIGURE 11. Unwrapped oil film thickness between piston/bushing interface over one revolution.

piston and deformation of piston and cylinder, the oil film thickness changes a lot in one revolution. From 90° to 270°, the displacement chamber enters low pressure area, and the maximum gap height is around 20μm. From 270° to 90°, the displacement chamber begins to discharge, and the maximum gap height can reach up to 25μm, that means the maximum deformation is around 5 μm.

The deformation of piston and cylinder plays an important role in the oil film gap height. Since the thickness of bushing has great effect to the deformation, it will finally affect the performance of oil film, such as the leakage flow and the viscous friction power loss.

B. LEAKAGE FLOW AND VISCOUS FRICTION POWER LOSS

The leakage flow rate for one piston cylinder interface with different bushing thicknesses is shown in Fig. 13. There are significant changes of leakage flow with the dynamic pressure in displacement chamber. With more bushing thickness, there will be more leakage flow. The deformation of bushing increases at larger bushing thickness, creating additional clearance between piston and cylinder. And finally the leakage flow increases.

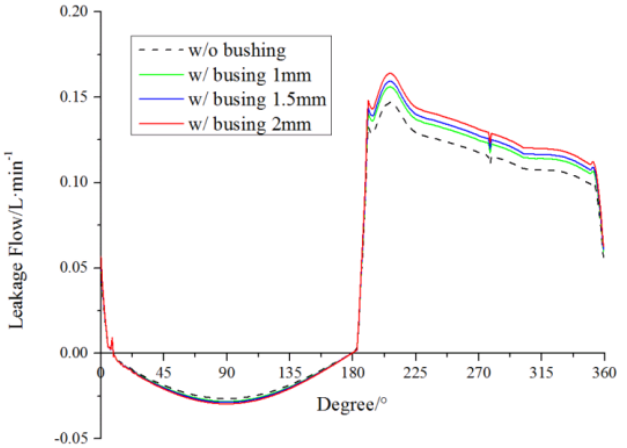

FIGURE 12. Leakage flow with different bushing thickness.

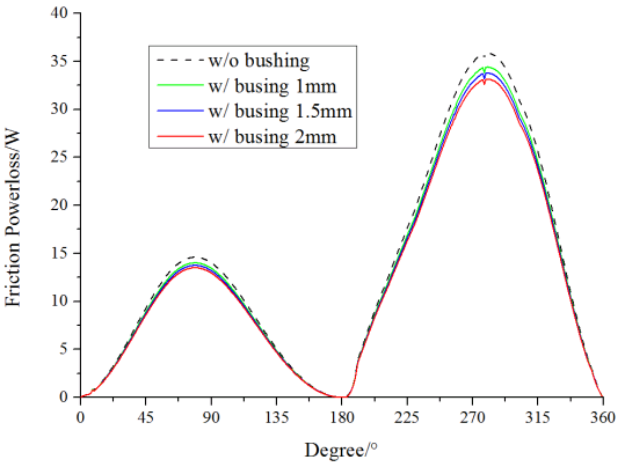

FIGURE 13. Viscous friction power loss with different bushing thickness.

The viscous friction power loss for one piston cylinder interface with different bushing thicknesses is shown in Fig. 13. The power loss decreases with the increasing of bushing thickness, especially in high pressure area. Since the clearance between piston and cylinder is increased with lager bushing thickness, the viscous force decreases.

C. EXPERIMENT RESULT

A viscous friction power loss test rig is built, which is shown in Fig. 14. The rotating shaft is driven by an electromotor. The swash plate is set to a tilt angle and rotate with drive shaft. With fluid pressure from hydraulic power station, the pistons are the pressure against the swash plate. The reciprocating motion of piston is realized under the fluid pressure and shaft rotation. Bushings with different thickness are prepared.

In order to eliminate the initial error of mechanical power loss, the test rig runs under small fluid pressure and the friction power loss of bearing block and couplings are measured. Experiments are performed under 35 MPa, 1500 rpm and 18° swashplate tilt angle. The average friction power losses of one piston/cylinder interface with different bushings are shown in Table 2.

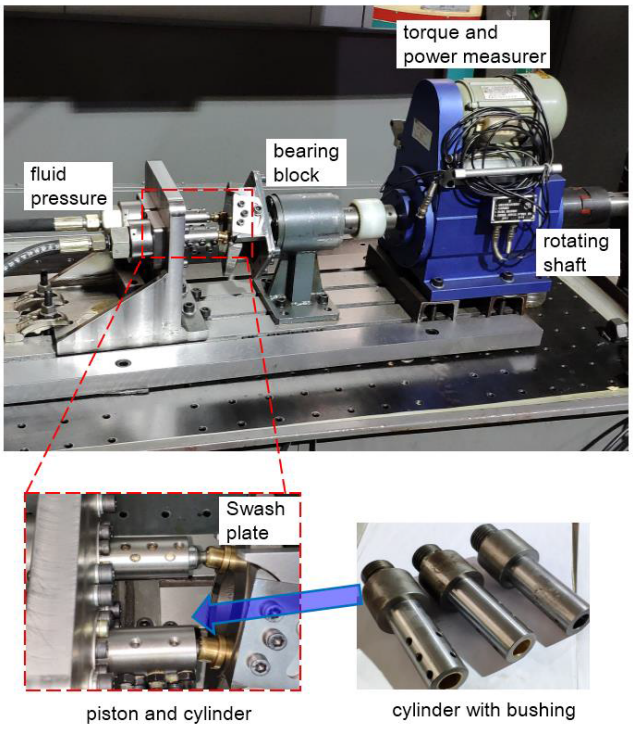

FIGURE 14. Viscous friction power loss test rig.

TABLE 2. Average leakage flow with different bushing thickness.

	Simulation		Experiment
	Avg. leakage flow ($L \cdot min^{-1}$)	Avg. friction power loss (W)	Avg. friction power loss (W)
w/o bushing	0.0485	13.568	14.1
w/ bushing 1mm	0.0512	13.014	13.6
w/ bushing 1.5mm	0.0525	12.776	13.3
w/ bushing 2mm	0.0540	12.540	13.0

The leakage flow with 2 mm bushing increases 11.52% comparing with the leakage flow without bushing. The viscous friction power loss with 2 mm bushing decreases 7.58% comparing with the power loss without bushing. The experimental results of friction power loss are similar to simulation results and shows the same variation tendency.

V. CONCLUSION

This paper presents a numerical model for piston/cylinder interface including piston pump main flow model and FSI model. The algorithm of the fluid and structure field is demonstrated, also with the dynamic interaction for those two fields. The results show that, there is non-negligible material deformation due to oil film pressure and contact. The deformation changes along with bushing thickness, and finally affects the performance of piston/cylinder interface. With the increasing of bushing thickness, the leakage flow rate will increase and the viscous friction power loss will decrease. With larger bushing thickness, there will be more deformation

and less pressure peaks which lead to more average gap height and less viscous friction force. The results highlight the model potentials to be used as a designing method for the axial piston pump to realize the optimal design for bushing thickness. Future developments of this study include optimal design of bushing thickness and importing the thermal effects in piston/cylinder interface model.

REFERENCES

[1] J. Yao, Z. Jiao, and D. Ma, "A practical nonlinear adaptive control of hydraulic servomechanisms with periodic-like disturbances," *IEEE/ASME Trans. Mechatronics*, vol. 20, no. 6, pp. 2752–2760, Dec. 2015.

[2] A. Yamaguchi, "Motion of the piston in piston pumps and motors—The case of metallic contact," *Trans. Jpn. Soc. Mech. Eng., B*, vol. 55, no. 518, pp. 3122–3128, 1989.

[3] R. M. Harris, K. A. Edge, and D. G. Tilley, "The spin motion of pistons in a swashplate-type axial piston pump," in *Proc. 3rd Scand. Int. Conf. Fluid Power*, Linköping, Sweden, 1993.

[4] K. Tanaka, K. Kyogoku, and T. Nakahara, "Lubrication characteristics on sliding surfaces between piston and cylinder in a piston pump and motor: Effects of running-in, profile of piston top and stiffness," *JSME Int. J. C Mech. Syst., Mach. Elements Manuf.*, vol. 42, no. 4, pp. 1031–1040, 1999.

[5] K. Tanaka, T. Nakahara, and K. Kyogoku, "Experimental verification of oil whirl of piston in axial piston pump and motor," *JSME Int. J. C Mech. Syst., Mach. Elements Manuf.*, vol. 44, no. 1, pp. 230–236, Mar. 2001.

[6] N. D. Manring, "Friction forces within the cylinder bores of swashplate type axial-piston pumps and motors," *J. Dyn. Syst., Meas., Control*, vol. 121, no. 3, pp. 531–537, 1999.

[7] Z. Li, R. Burton, and P. Nikiforuk, "Experimental simulation of piston leakage in an axial piston pump," in *Proc. ASME Fluid Power Syst. Technol.*, vol. 12, 2005, pp. 9–15.

[8] U. Wieczorek and M. Ivantysynova, "Computer aided optimization of bearing and sealing gaps in hydrostatic machines—The simulation tool caspar," *Int. J. Fluid Power*, vol. 3, no. 1, pp. 7–20, 2002.

[9] M. Pelosi and M. Ivantysynova, "A novel fluid-structure interaction model for lubricating gaps of piston machines," in *Proc. 5th Fluid Struct. Interact. Conf.*, vol. 105, 2009, pp. 13–20.

[10] M. Pelosi and M. Ivantysynova, "A geometric multigrid solver for the piston–cylinder interface of axial piston machines," *Tribology Trans.*, vol. 55, no. 2, pp. 163–174, 2012.

[11] M. Pelosi and M. Ivantysynova, "Surface deformations enable high pressure operation of axial piston pumps," in *Proc. ASME Dyn. Syst. Control Conf. BATH/ASME Symp. Fluid Power Motion Control*, vol. 1, 2012, pp. 193–200.

[12] S. Kumar and J. M. Bergada, "The effect of piston grooves performance in an axial piston pumps via CFD analysis," *Int. J. Mech. Sci.*, vol. 66, pp. 168–179, Jan. 2013.

[13] B. Xu, J. Zhang, and H. Yang, "Simulation research on distribution method of axial piston pump utilizing pressure equalization mechanism," *Proc. Inst. Mech. Eng., C, J. Mech. Eng. Sci.*, vol. 227, no. C3, pp. 459–469, 2013.

[14] B. Xu, J. Zhang, H. Yang, and B. Zhang, "Investigation on the radial micromotion about piston of axial piston pump," *Chin. J. Mech. Eng.*, vol. 26, no. 2, pp. 325–333, Mar. 2013.

[15] J. Jiang and K. Wang, "An integrated model of hydrodynamic lubricating for piston/cylinder interface," in *Proc. Int. Conf. Fluid Power Mechatron. (FPM)*, Aug. 2015, pp. 47–52.

[16] A. M. Wondergem and M. Ivantysynova, "The impact of the surface shape of the piston on power losses," in *Proc. 8th FPNI Ph.D Symp. Fluid Power*, 2014, Art. no. V001T02A008.

[17] A. M. Wondergem and M. Ivantysynoya, "The impact of micro-surface shaping on the piston/cylinder interface of swash plate type machines," in *Proc. ASME/BATH Symp. Fluid Power Motion Control*, 2015, Art. no. V001T01A060.

[18] B. J. Hamrock, S. R. Schmid, and B. O. Jacobson, *Fundamentals of Fluid Film Lubrication*, 2nd ed. New York, NY, USA: Marcel Dekker, 2004, pp. 181–204.

[19] J. Ivantysyn and M. Ivantysynova, *Hydrostatic Pumps and Motors*. New Delhi, India: Akademia Books International, 2001.

[20] H. Jasak and H. G. Weller, "Application of the finite volume method and unstructured meshes to linear elasticity," *Int. J. Numer. Methods Eng.*, vol. 48, pp. 267–287, 2000.

JIANG JIHAI was born in 1957. He received the Ph.D. degree in mechanical engineering from the Harbin Institute of Technology, Harbin, China, in 1999.

He is currently a Professor with the School of Mechatronics Engineering, Harbin Institute of Technology. He has conducted several projects from the National Nature Science Foundation, two projects from the National Key Technology R&D Program. His current research interests include new type hydraulic components, advanced design technology, energy saving technology, and reliability research of hydraulic components.

WANG KELONG was born in 1985. He received the M.S. degree in mechanical engineering from the Harbin Institute of Technology, Harbin, China, in 2011.

He is currently pursuing the Ph.D. degree in mechanical engineering with the Harbin Institute of Technology, mainly engaged in modeling and optimization of hydraulic components, and computer simulation design. From 2013 to 2015, he was a Visiting Ph.D. Student with the Maha Fluid Power Research Center, Lafayette, IN, USA.

WANG ZEBO was born in 1986. He received the M.S. degree in mechatronic engineering from the Kunming University of Science and Technology, Kunming, China, in 2012.

He is currently pursuing the Ph.D. degree in mechanical engineering with the Harbin Institute of Technology, mainly engaged in modeling and optimization of hydraulic components, and computer simulation design.

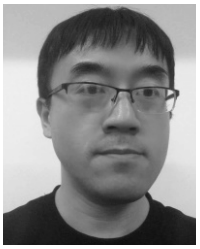

SUN YI was born in 1979. He received the Ph.D. degree in mechanical engineering from the Harbin Institute of Technology, Harbin, China, in 2013.

He is currently an Engineer with the Beijing Institute of Precision Mechatronics and Control Equipment, mainly focus on the control and optimal design on hydraulic systems.